

Longformer: Longitudinal Transformer for Alzheimer’s Disease Classification with Structural MRIs

Qiuhui Chen¹ and Yi Hong^{1*}

¹Department of Computer Science and Engineering, Shanghai Jiao Tong University, China
yi.hong@sjtu.edu.cn

Abstract

Structural magnetic resonance imaging (sMRI) is widely used for brain neurological disease diagnosis; while longitudinal MRIs are often collected to monitor and capture disease progression, as clinically used in diagnosing Alzheimer’s disease (AD). However, most current methods neglect AD’s progressive nature and only take a single sMRI for recognizing AD. In this paper, we consider the problem of leveraging the longitudinal MRIs of a subject for AD identification. To capture longitudinal changes in sMRIs, we propose a novel model Longformer, a spatiotemporal transformer network that performs attention mechanisms spatially on sMRIs at each time point and integrates brain region features over time to obtain longitudinal embeddings for classification. Our Longformer achieves state-of-the-art performance on two binary classification tasks of separating different stages of AD using the ADNI dataset. Our source code is available at <https://github.com/Qybc/LongFormer>.

1 Introduction

Alzheimer’s Disease (AD) is one of the most common cognitive impairment diseases suffered by older people. Medical brain scans, like Magnetic Resonance Images (MRIs) provide a non-invasive way to capture disease pathological patterns and have the potential to help doctors make an early diagnosis before physical symptoms appear. As shown by an extreme case in Fig. 1(a) to compare MRI scans of normal control (NC) and AD subjects, the AD one typically shows enlarged ventricles and hippocampus and shrinking cerebral cortex. However, one single MRI is not enough to distinguish them correctly. In clinical diagnosis, the degeneration speed inferred from the followed-up/longitudinal image scans is an important factor for recognizing AD subjects [Saboo *et al.*, 2021; Qiu *et al.*, 2022]. We can also observe this as demonstrated in Fig. 1(b). By only considering the appearance of each MRI independently, we would make the wrong separation between these two subjects. However, if we consider the changes between baselines and their follow-up scans, it becomes much easier to separate them. Therefore, leveraging

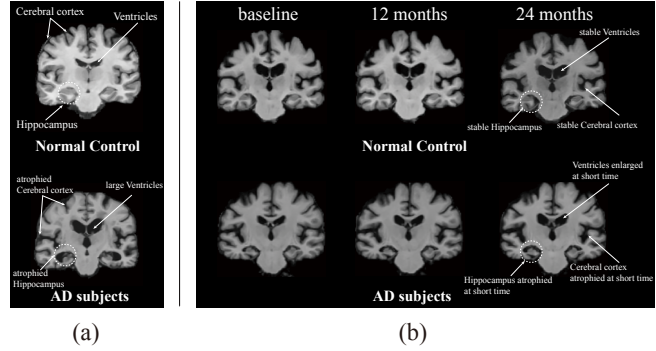


Figure 1: Illustration of the difference between normal controls and AD subjects. (a) a single sMRI and (b) longitudinal sMRIs.

the longitudinal brain MRIs is a promising way for studying AD and helping computer-aided AD diagnosis.

In this paper, we consider learning from 3D longitudinal structural MRIs (sMRIs) to separate AD subjects from normal controls and to separate progressive mild cognitive impairment (pMCI) from stable MCI (sMCI), in an end-to-end network fashion. Researchers have collected brain MRI scans of a subject at multiple time points, resulting in a longitudinal dataset for tracking the progression of AD, e.g., the well-known ADNI dataset [Jack Jr *et al.*, 2008]. However, most current methods proposed for MRI-based AD diagnosis treat their used datasets as cross-sectional ones [Jang and Hwang, 2022; Zhu *et al.*, 2021], that is, they simply consider a single MRI for classification but ignore the degeneration progress included in the MRI sequence of a subject. Limited work has been done to fully leverage the longitudinal dataset [Cui *et al.*, 2019]. A recent work proposed in [Hu *et al.*, 2023] considers only two time points for studying AD.

To handle longitudinal image sequences, we turn to Transformer, since it has been successfully used in analyzing both language and image sequences [Vaswani *et al.*, 2017]. To consider the MRI sequence as a whole for classification, we treat the longitudinal AD diagnosis as a problem of set prediction, similar to DETR proposed in [Carion *et al.*, 2020]. One of the challenging tasks in analyzing longitudinal MRIs is how to capture the subtle brain structure changes in the MRI sequence, which are beneficial for classification. To address this problem, we adopt the 3D version of the deformable

attention mechanism proposed in [Zhu *et al.*, 2020], which is able to reduce model computational complexity. Based upon these techniques, we propose a model named Longformer that uses a CNN backbone and a transformer encoder to extract feature embeddings from MRIs and a longitudinal transformer decoder to integrate spatiotemporal embedding information for the final AD classification.

In summary, our contributions in this paper are three-fold:

- To our best knowledge, we are the first to explore an efficient vision Transformer on 3D longitudinal image volumes, which adaptively extracts spatiotemporal features, especially the degeneration progress from a longitudinal perspective for Alzheimer’s disease classification.
- We propose a novel model Longformer based on spatiotemporal queries for collecting longitudinal 3D MRI features and object queries for 4D integration. These queries are decomposed into a target query and other helper queries, whose effectiveness is visually shown.
- Our Longformer achieves the state-of-the-art (SOTA) performance (97%~98% accuracy) on two classification tasks, i.e., AD vs. NC and pMCI vs. sMCI, using the largest set of the ADNI database with 1840 subjects.

2 Related Work

Vision Transformer. Transformer is firstly proposed for the sequence-to-sequence machine translation [Vaswani *et al.*, 2017] and currently becomes the basic component in most Natural Language Processing tasks. Recently, Transformer has been successfully applied in computer vision, such as DETR [Carion *et al.*, 2020] for object detection, SETR [Zheng *et al.*, 2021] for semantic segmentation, ViT [Dosovitskiy *et al.*, 2020] and DeiT [Touvron *et al.*, 2021] for image recognition. DETR proposes a new detection paradigm upon transformers, which simplifies the object detection to a set prediction problem. Deformable DETR [Zhu *et al.*, 2020] achieves better performance by using local attention and multi-scale feature maps. To handle videos, which are sequences of image frames, SeqFormer [Wu *et al.*, 2022] proposed to adopt Deformable DETR in the video instance segmentation task. SeqFormer proposes the query decomposition mechanism, splits instance queries at each frame, and then aggregates them to obtain a representation at the video level. We share the same motivation; differently, we use a fixed number of object queries with one as the target query, while others are helpers to figure out “where to look at”.

CNN-Based AD Classification. Deep neural networks have been widely applied for AD recognition. Thanks to publicly-available large datasets, like ADNI and AIBL [Rowe *et al.*, 2010], training deep models for detecting AD pathology becomes possible. In 2018, a hierarchical fully convolutional network (FCN) is proposed in [Lian *et al.*, 2018] to learn multi-scale features from both small patches and whole brain regions to perform AD diagnosis. In 2020, a multimodality FCN with a multilayer perceptron (MLP) model is proposed in [Qiu *et al.*, 2020] to take both MRIs and the corresponding subject attributes (e.g., age, gender) and is trained on ADNI and tested on multiple datasets including AIBL,

National Alzheimer’s Coordinating Center (NACC) and the Framingham Heart Study (FHS). In 2021, a dual-attention multi-instance deep learning model (DA-MIDL) is proposed in [Zhu *et al.*, 2021] to identify discriminative pathological locations for AD diagnosis using structural MRIs.

Recently in 2022, a three-dimensional medical image classifier is proposed in [Jang and Hwang, 2022], using a multi-plane and multi-slice Transformer (M3T) network to classify Alzheimer’s disease (AD) using 3D MRI images. The proposed network synergically combines 3D CNN, 2D CNN, and Transformer for AD classification. A 3D Global Fourier Network (GF-Net) is proposed in [Zhang *et al.*, 2022] to utilize global frequency information that captures long-range dependency in the spatial domain. Another work called Trans-ResNet is proposed in [Li *et al.*, 2022] to integrate CNNs and Transformers for AD classification.

Different from these existing works that only consider cross-sectional (i.e., a single image data point, ignoring time information) MRI scans, our model captures longitudinal changes in MRI sequences, which is an important feature for degenerative diseases, such as AD.

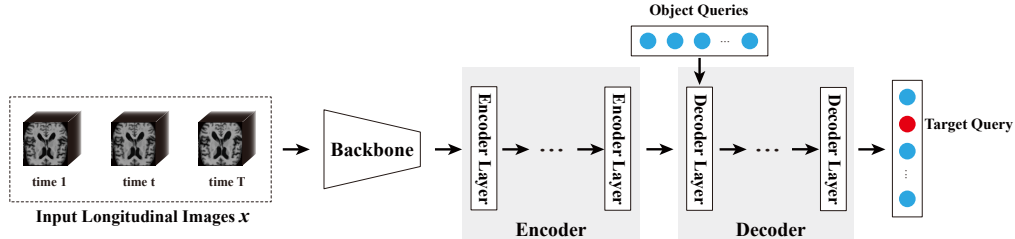
Longitudinal Analysis for Image-Based AD Study. Longitudinal study tracks the changes in brain morphology of AD subjects over time. Different from the cross-sectional setting, the longitudinal one considers multiple images from the same subject scanned at different time points as a whole for analysis. This means the dimension of the input data increases while the number of training samples decreases, which brings the risk of overfitting, especially for 3D medical image volumes. To address this issue, researchers use a 3D CNN to extract brain image features from each MRI, and an RNN to fuse these features to extract the longitudinal change information [Cui *et al.*, 2019]. A recent work [Hu *et al.*, 2023] extracts features from longitudinal sMRI image slices, i.e., the baseline and its follow-up scan, and encodes them as high-level feature representation tokens by using a transformer. Since this method takes only 2D slices and two time points, it losses both spatial and temporal information of a subject in the original ADNI dataset. Different from these methods, we work on 3D MRI volumes at multiple time points and adopt efficient attention mechanisms to extract spatiotemporal embeddings, resulting in the best performance compared to all existing methods.

3 Methodology

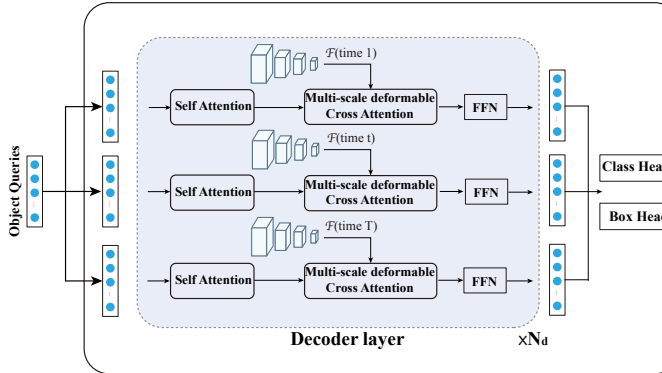
Figure 2 presents the overview of our proposed method, including a backbone and a transformer encoder to obtain multi-scale feature embeddings and a transformer decoder for integrating longitudinal embeddings with object queries and outputting the final classification prediction.

3.1 Backbone and Transformer Encoder

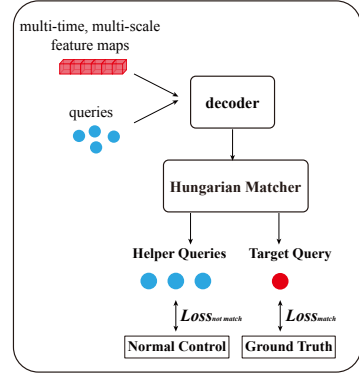
We use UNet3D [Shapey *et al.*, 2019] as the network backbone to extract multi-scale features from input images. In particular, the backbone takes a longitudinal input $\mathbf{x} \in \mathbb{R}^{T \times 1 \times H \times W \times D}$, which includes multiple grayscale images (one channel) of resolution $H \times W \times D$ collected at T time points. As shown in Fig. 3, multi-scale feature maps $\{\mathcal{F}_l\}_{l=1}^L$



(a) Overview of our method Longformer.



(b) Longitudinal Transformable Decoder.



(c) Helper Query Strategy

Figure 2: Illustration of our proposed Longformer. FFN: Feed-Forward Network.

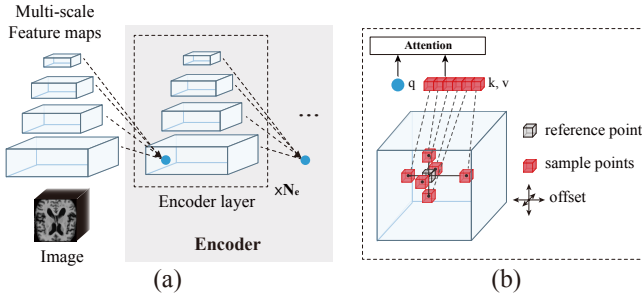


Figure 3: Illustration of the backbone and a transformer encoder. (a) Multi-scale self-attention in the encoder, where dashed arrows indicate deformation attention. (b) Details of deformable attention.

$(L = 4)$ are collected from the upsampling feature maps of blocks B_2 through B_5 in UNet3D. The dimension of all feature maps is reduced to $C = 288$ by applying a 1×1 convolution. We extract such feature maps for images at each time point independently, resulting in a set of feature maps $\{\{\mathcal{F}_t\}_{l=1}^L\}_{t=1}^T$ with different resolutions, which is followed by a feature embedding via a transformer encoder, as shown in Fig. 2(a).

In the transformer encoder, we add the fixed positional encodings [Carion *et al.*, 2020] to each scale of the extracted feature maps, which is flatten and concatenated together to obtain a feature vector. Then a multi-scale deformable attention (MSDA) [Zhu *et al.*, 2020] is adopted to perform attention mechanisms spatially. To avoid mixing the spatial and

temporal features, we perform transformer embedding independently for each time point, resulting in the feature maps $\{\mathcal{F}_t^{ms}\}_{t=1}^T$ as the output of this transformer encoder.

3.2 Longitudinal Transformer Decoder

Given an sMRI with follow-up scans, experts can recognize important regions related to AD and identify longitudinal changes in the brain morphogenesis of a subject. That is, the experts treat the same region at different time points as a whole for consideration and obtain changes over time through comparison among image time series. This is the main difference between models based on a single sMRI and those based on longitudinal sMRIs. To simulate this, we propose a longitudinal transformer decoder to learn a spatiotemporal representation across image time series.

To obtain the longitudinal feature embeddings, in the transformer decoder we propose to use object queries, which are learnable embeddings containing integrated spatiotemporal information. We set N_q object queries and each is a vector of size L_q , which is represented in a matrix form \mathbf{O}^q with the size of $L_q \times N_q$, and each column is an object query. To incorporate both spatial and time information into the object queries, we need $T \times N_q$ helpers, that is, we need T spatiotemporal queries $\{\mathbf{ST}_t^q\}_{t=1}^T$ in the matrix form, which has the same spatial size of \mathbf{O}^q . Each of these spatiotemporal queries serves as an anchor for retrieving and locating features on the corresponding time point. By using these time-specific queries, we can better align the brain region and perform deformable attention within the foreground via an additional bounding-box prediction branch of the brain region.

In particular, we start with the object queries at the first decoder layer \mathbf{O}_1^q , which are used to query the region features on features maps at each time point independently:

$$\mathbf{ST}_{1,t}^q = \text{DeformAttn}(\mathbf{O}_1^q, \mathcal{F}_t^{ms}), \quad (1)$$

where $\mathbf{ST}_{1,t}^q$ represents the spatiotemporal queries at the time point t obtained at the 1st decoder layer. The function DeformAttn indicates the deformable attention module used in [Zhu *et al.*, 2020]. Given a query element \mathbf{O}_1^q at the same layer and the feature maps \mathcal{F}_t^{ms} , the deformable attention only explores a small set of key sampling points, as shown in Fig. 3. For the following decoder layers, e.g., the l -th ($l > 1$) layer, we update the spatiotemporal queries $\mathbf{ST}_{l,t}^q$ from their old queries at the last layer $l - 1$:

$$\mathbf{ST}_{l,t}^q = \text{DeformAttn}(\mathbf{ST}_{l-1,t}^q, \mathcal{F}_t^{ms}). \quad (2)$$

Based upon the spatiotemporal queries, the object queries aggregate the temporal features by a weighted sum of all spatiotemporal queries at the end of each decoder layer:

$$\mathbf{O}_q^l = \frac{\sum_{t=1}^T \mathbf{ST}_t^l \times \text{FC}(\mathbf{ST}_t^l)}{\sum_{t=1}^T \text{FC}(\mathbf{ST}_t^l)} + \mathbf{O}_q^{l-1}. \quad (3)$$

Here, FC indicates the fully connected layer, which is used to generate the weights for averaging the spatiotemporal queries at the same layer. At the last layer of the transformer decoder, we obtain the object queries \mathbf{O}_q^q , summarizing the spatiotemporal information from all images at each time point, and the spatiotemporal queries \mathbf{ST}_t^q at T time points. As shown in Fig. 2(c), among these queries, we take one as the *target query* and the rest as the *helper queries*. In the following Section 3.3, we will discuss how to decompose the object queries into these two categories.

Output Heads. As shown in Fig 2(b), we add a box head and a class head on the top of the transformer decoder outputs. A linear projection acts as the class head to produce the classification result. Given the N_q spatiotemporal feature embeddings, i.e., \mathbf{O}_q^q , from the transformer decoder and each with an index σ_i , the class head outputs a class probability of a class for each embedding, which is $\hat{p}_{\sigma_i}(c_i)$ and annotated as \hat{c}_{σ_i} . On the other hand, the box head is a three-layer feed-forward network (FFN) with a ReLU activation function and a linear projection layer. For \mathbf{ST}_t^q at each time point, the FFN predicts the normalized center coordinates, height, and width of the bounding box of the brain region at time point t . Thus, for the brain with the index σ_i , we denote the predicted box sequence as $\hat{\mathbf{B}}_{\sigma_i} = \{\hat{\mathbf{b}}_{(\sigma_i,1)}, \hat{\mathbf{b}}_{(\sigma_i,2)}, \dots, \hat{\mathbf{b}}_{(\sigma_i,T)}\}$. As a result, the output heads produce N_q predictions $\hat{\mathbf{y}}_i = \{\hat{c}_{\sigma_i}, \hat{\mathbf{B}}_{\sigma_i}\}_{i=1}^{N_q}$.

3.3 Query Matching and Loss Functions

To explore more regions of the images, we typically set the object query number N_q significantly big, which is much larger than what we need for the final classification. Therefore, we need to find a bipartite graph matching between the network predictions $\hat{\mathbf{y}} = \{\hat{\mathbf{y}}_i\}_{i=1}^{N_q}$ and our ground truth labels y . For the input image sequence, we have one class label c , e.g., NC or AD, and the bounding box labels at each

time point $\mathbf{b} = \{b_t\}_{t=1}^T$, and each b_t represents a vector that defines ground truth bounding box center coordinates and its relative height and width at the time-point t . That is, $y = \{c, b_1, b_2, \dots, b_T\}$. We would like to find the best match indexed as σ_i in $\hat{\mathbf{y}}$ with the ground truth y , which gives us the target query. Thus, we define the pair matching cost between ground truth y and a prediction with the index σ_i :

$$\mathcal{L}_{\text{match}}(y, \hat{\mathbf{y}}_{\sigma_i}) = \mathcal{L}_{\text{cls}}(c, \hat{c}_{\sigma_i}) + \mathcal{L}_{\text{box}}(\mathbf{b}, \hat{\mathbf{b}}_{\sigma_i}) \quad (4)$$

where \hat{c}_{σ_i} is the predicted target class label. For those not-matched queries, i.e., our helper queries, we define the unpaired matching cost:

$$\mathcal{L}_{\text{not-match}}(y, \hat{\mathbf{y}}_{\sigma_j}) = \sum_{j \neq i}^{N_q} (\mathcal{L}_{\text{cls}}(c_j, \hat{c}_{\sigma_j}) + \mathcal{L}_{\text{box}}(\mathbf{b}, \hat{\mathbf{b}}_{\sigma_j})) \quad (5)$$

where c_j is set as the NC label (AD vs. NC) or the sMCI label (pMCI vs. sMCI) to let helper queries collect desired information for classification from NC or sMCI subjects.

To find the best assignment of ground truth to a query's prediction, we search among the permutation of N_q elements, i.e., $\sigma \in S_n$ and find the one with the lowest cost:

$$\hat{\sigma} = \arg \min_{\sigma \in S_n} \sum_{i=1}^{N_q} \mathcal{L}_{\text{match}}(y, \hat{\mathbf{y}}_{\sigma_i}). \quad (6)$$

Following the previous works [Zhu *et al.*, 2020; Carion *et al.*, 2020], the optimal solution is computed with the Hungarian algorithm. Given the optimal assignment $\hat{\sigma}$, we use Hungarian loss for all n matched pairs to train the network:

$$\mathcal{L}_{\text{Hung}}(y, \hat{\mathbf{y}}) = \sum_{i=1}^n [\mathcal{L}_{\text{cls}}(c, \hat{c}_{\hat{\sigma}_i}) + \mathcal{L}_{\text{box}}(\mathbf{b}, \hat{\mathbf{b}}_{\hat{\sigma}_i})]. \quad (7)$$

For \mathcal{L}_{cls} , we use a sigmoid focal loss [Lin *et al.*, 2017] for the non-matched set and cross-entropy loss for the matched one. For \mathcal{L}_{box} , we use a linear combination of the L_1 loss and the generalized IoU loss [Rezatofighi *et al.*, 2019].

4 Experiments

4.1 Dataset, Baselines and Evaluation Metrics

To evaluate our model, we use the public Alzheimer's Disease Neuroimaging Initiative (ADNI) dataset [Jack Jr *et al.*, 2008]. This dataset includes 8016 1.5T/3T T1-weighted structural MRI (sMRI) scans collected from 1840 subjects with visits at one or multiple time points across four ADNI phases (i.e., ADNI-1, ADNI-2, ADNI-GO and ADNI-3). These subjects can be divided into three categories: AD (Alzheimer's disease), MCI (mild cognitive impairment), and NC (normal control) in accordance with the standard clinical criteria, e.g., the Mini-Mental State Examination (MMSE) scores and the Clinical Dementia Rating (CDR). For MCI conversion prediction, MCI subjects can be further divided into two sub-categories: pMCI (progressive MCI) subjects who have converted to AD within 36 months after their baseline visits and sMCI (stable MCI) subjects who are still diagnosed as MCI 36 months later). Therefore, we have 381 AD, 637 NC, 278 pMCI, and 544 sMCI subjects for our following experiments.

Modeling Type	Method	# Subjects				AD vs. NC		pMCI vs. sMCI	
		AD	NC	pMCI	sMCI	Accuracy	AUC	Accuracy	AUC
Single sMRI	[Eskildsen <i>et al.</i> , 2013]	194	226	61	134	0.867	0.917	0.773	0.835
	[Tong <i>et al.</i> , 2014]	198	231	167	238	0.900	-	0.720	-
	[Cao <i>et al.</i> , 2017]	192	229	168	229	0.886	0.898	0.704	0.705
	wH-FCN [Lian <i>et al.</i> , 2018]	358	429	205	465	0.90	0.95	0.81	0.78
	[Lin <i>et al.</i> , 2018]	188	229	169	139	0.888	-	0.799	0.861
	[Li <i>et al.</i> , 2018]	199	229	-	-	0.895	0.924	-	-
	[Qiu <i>et al.</i> , 2020]	188	229	-	-	0.834	-	-	-
	DA-MIDL [Zhu <i>et al.</i> , 2021]	389	400	172	232	0.924	0.965	0.802	0.851
	Trans-ResNet [Li <i>et al.</i> , 2022]	197	366	-	-	0.939	0.968	-	-
	GFNet [Zhang <i>et al.</i> , 2022]	188	229	-	-	0.941	0.935	-	-
Longitudinal sMRIs	M3T [Jang and Hwang, 2022]	242	509	-	-	0.9321	0.9634	-	-
	Longformer-S (ours)	381	637	278	544	0.9618	0.9811	0.9292	0.9320
	[Cui <i>et al.</i> , 2019]	198	229	167	236	0.9133	0.9322	0.7171	0.7303
Longitudinal sMRIs	VGG-TSwinformer [Hu <i>et al.</i> , 2023]	-	-	121	154	-	-	0.7720	0.8153
	Longformer-L (ours)	268	364	254	388	0.9823	0.9718	0.9687	0.9710

Table 1: Classification comparison between our methods with baselines on the ADNI dataset, including AD and NC classification and MCI conversion prediction, i.e., pMCI versus sMCI. The **bold red** color indicates the best performance, and the **blue** color indicates the second best. Some items are unfilled because those values are missing in the original papers.

The original structural MRI data downloaded from the ADNI website went through a series of pre-processing steps, including denoising, bias field correction, skull stripping, and affine registration to the SRI24 atlas. Then, we resize the image volumes, resulting in images of size $128 \times 128 \times 128$, with a resolution of $1.75mm \times 1.75mm \times 1.75mm$. Lastly, we normalize the image intensity to zero mean and unit variance. After pre-processing, we perform two tasks: (1) classifying AD and NC, and (2) classifying pMCI and sMCI. To evaluate the classification performance, we use the classification accuracy (ACC) and the area under receiver operating characteristic curve (AUC) as our evaluation metrics.

We compare our Longformer method with two groups of baselines, including 11 existing methods using a single sMRI and two methods using longitudinal-sMRIs, as shown in Table 1. To compare with the first group of baselines, we degrade our method to handle just one time point, i.e., $T = 1$, which is named Longformer-S. We simply choose the first scan of all subjects, i.e., the baseline scan, for this experiment. For the second group comparison, we apply our method to handle three time points, $T = 3$, starting with the baseline scan, then 6 and 12 months, which is named Longformer-L. Since some subjects have less than three time points, we ignore them from the second comparison, resulting in 268 AD, 364 NC, 254 pMCI, and 388 sMCI subjects for evaluation.

We report our experimental results under the five-fold cross-validation setting. For other baseline methods, we take the corresponding values from their papers, since it is unclear how to select the subset from ADNI to reproduce their results. However, among all methods, our method is evaluated on the largest ADNI subset.

4.2 Implementation Details and Experimental Settings

We apply a 3D UNet as our CNN backbone. This UNet takes image volumes of size $128 \times 128 \times 128$ and converts them

into 3D representation features with 288 channels. We set the sampled key numbers $K = 4$ and six attention heads for deformable attention modules. We use six encoder and six decoder layers with a hidden dimension of 288 for the transformer, and the number of object queries N_q is set as 300.

We use the AdamW optimizer with a learning rate of 2e-4, $\beta_1 = 0.9$, $\beta_2 = 0.999$, and weight decay of 1e-4. The learning rate decays at the 6th and 10th epochs by a factor of 0.1. Our model is implemented using PyTorch-1.12 and is trained on four NVIDIA GeForce RTX 3090 GPUs, with three MRI scans per GPU.

4.3 Experimental Results and Ablation Study

Table 1 presents the comparison results between our Longformer models with 13 baselines using either a single sMRI or longitudinal sMRIs. Our Longformer-L and Longformer-S rank in the first and second places for both classification tasks, i.e., AD vs. NC and pMCI vs. sMCI. The improvement of Longformer-L over Longformer-S demonstrates the necessity of using longitudinal data for AD classification. Also, our Longformer-L improves all evaluation metrics by approximately or over 0.97, which are never achieved before. Also, our Longformer-L outperforms existing methods by a good margin, especially for classifying pMCI and sMCI, which improves the SOTA by approximately 16% in classification accuracy and 11% in AUC.

Query Analysis. Object queries, especially the part of helper queries, play an important role in our model. We would like to answer two questions: (1) How do queries/helper queries contribute to the AD study? and (2) How many queries/helper queries are desired for a good classification result?

Figure 4 visualizes the target query (in red) and the helper queries (in green) of some sample points. Each query has a fixed number of learnable sample points for deformable attention. We visualize these queries via three views of an image volume, i.e., coronal, axial, and sagittal planes. As we ob-

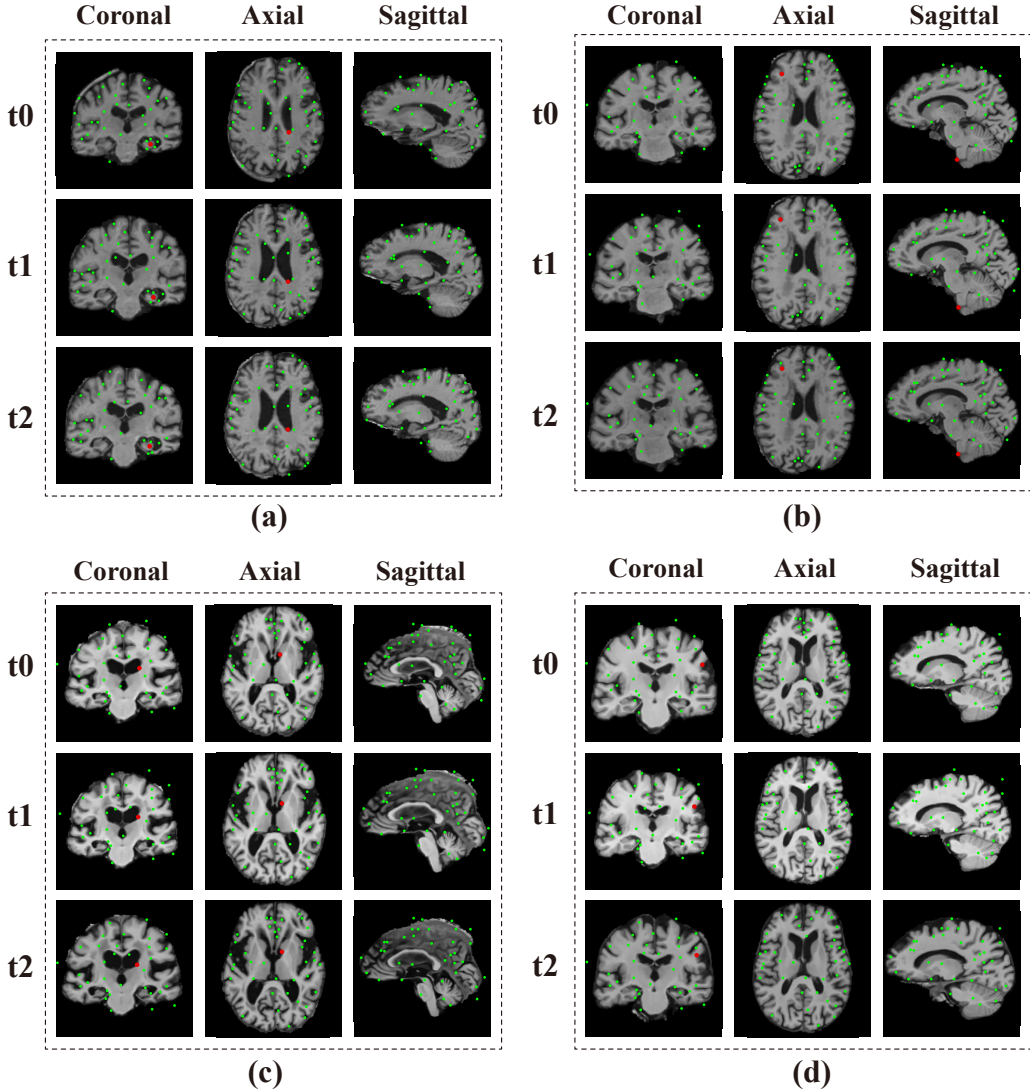


Figure 4: Visualization of object queries from the last decoder layer. (a) AD, (b) NC, (c) progressive MCI (pMCI), and (d) stable MCI (sMCI). Sample points of helper queries are in green and those of target queries are in red. (Best viewed in color)

serve from Fig. 4(b) and (d), if the target query has the same label as helper queries, they share similar behaviors of “looking at” MRI scans, i.e., focusing on the boundaries of brain structures. If the target query has a different label with helper queries, the target query pays more attention to brain structures that are greatly affected by Alzheimer’s disease, such as the hippocampus and ventricles shown in Fig. 4(a) and (c). For all cases, helper queries are well distributed within the brain regions to extract their features over time. Please see the supplementary material for more visualization results.

Table 2 demonstrates the necessity of using more helper queries. The model with just one query, i.e., one target query and no helper queries, fails to distinguish AD subjects from normal controls. As the number of helper queries increases, the classification performance improves accordingly and then saturates once we have 100 queries, i.e., including 99 helper queries. With more helper queries, e.g., 300 queries including

299 helper queries, the classification performance remains the same; however, we observe that the model converges faster than the one using 100 queries.

Longitudinal Information Helps. Table 3 presents the performance improvement of our model by using different numbers of time points on the classifications of AD vs. NC and pMCI vs. sMCI. Here, t_0 , t_1 , and t_2 denote the baseline, 6 months, and 12 months, respectively. As we can see, the classification performances gradually improve when adding more sequential data as the longitudinal inputs, indicating the necessity of using longitudinal MRIs for AD diagnosis.

Box Head Also Helps. The bounding-box prediction of the brain region via the box head is an auxiliary task of our model. Table 4 demonstrates the necessity of using this output branch. Without the bounding-box prediction, the classification performance drops significantly. Visually, more sample points are distributed outside the brain, as shown in the top

Query numbers	AD vs. NC		pMCI vs. sMCI	
	Accuracy	AUC	Accuracy	AUC
1	0.2419	0.5000	0.2037	0.5000
2	0.2419	0.5000	0.2037	0.5000
10	0.9203	0.9222	0.9027	0.9026
20	0.9646	0.9660	0.9558	0.9579
100	0.9823	0.9718	0.9687	0.9710
300	0.9823	0.9718	0.9687	0.9710

Table 2: Experiments on query numbers and their effects on the classification performance.

Time Points	AD vs. NC		pMCI vs. sMCI	
	Accuracy	AUC	Accuracy	AUC
$\{t_0\}$	0.9618	0.9811	0.9292	0.9320
$\{t_0, t_1\}$	0.9735	0.9741	0.9381	0.9418
$\{t_0, t_1, t_2\}$	0.9823	0.9718	0.9687	0.9710

Table 3: Performance comparison between longitudinal sMRIs with different numbers of time points.

row of Fig. 5. While with the box head, the deformable attention would be forced to focus on the brain region, leaving few helper queries outside of the brain area (see the bottom row of Fig. 5). This box head also helps alleviate the misalignment issue of MRIs at different time points.

5 Conclusion

In this paper, we have proposed an effective transformer architecture, Longformer, for Alzheimer’s Disease Classification based on longitudinal sMRI volumes. Longformer performs attention mechanisms at all time points using the proposed spatiotemporal queries and integrates their features into the shared powerful object queries, which include a target query for the final prediction and other helper queries assisting the target query. Our Longformer is an end-to-end framework for separating AD from NC and separating pMCI from sMCI, with no limit on the length of image time series. Our model achieves the SOTA classification performance on the largest set of the ADNI dataset.

Limitations and Future Work. Our experiments focus on binary classification, which could be extended to multi-label classification, e.g., classifying AD, MCI, and NC. Besides, our model cannot handle subjects with missing time points, which is left for our future work. Also, our Longformer only takes MRI scans for AD classification; while other attributes, like age, gender, and lab results, are also beneficial for AD diagnosis. In future work, we will integrate these attributes into our model to further improve classification accuracy. Besides, our model works on a single modality, i.e., sMRI, other modalities, like PET, fMRI, etc., could be also taken into account for AD study. Building a multi-modal AD classifier will be left for future work as well.

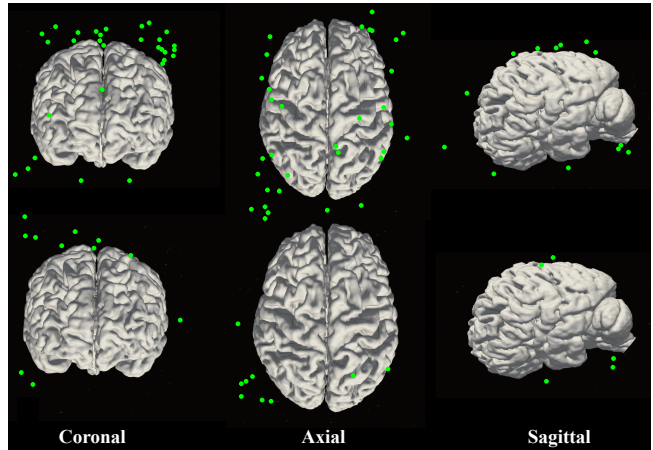


Figure 5: Visualization of sample points corresponding to helper queries (green points) without (top) and with (bottom) the box head.

Box Head	AD vs. NC		pMCI vs. sMCI	
	Accuracy	AUC	Accuracy	AUC
w/o	0.2419	0.5000	0.2037	0.5000
w	0.9823	0.9718	0.9687	0.9710

Table 4: Classification performance comparison without (w/o) and with (w) the box head.

References

- [Cao *et al.*, 2017] Peng Cao, Xiaoli Liu, Jinzhu Yang, Dazhe Zhao, Min Huang, Jian Zhang, and Osmar Zaiane. Nonlinearity-aware based dimensionality reduction and over-sampling for ad/mci classification from mri measures. *Computers in biology and medicine*, 91:21–37, 2017.
- [Carion *et al.*, 2020] Nicolas Carion, Francisco Massa, Gabriel Synnaeve, Nicolas Usunier, Alexander Kirillov, and Sergey Zagoruyko. End-to-end object detection with transformers. In *European conference on computer vision*, pages 213–229. Springer, 2020.
- [Cui *et al.*, 2019] Ruoxuan Cui, Manhua Liu, Alzheimer’s Disease Neuroimaging Initiative, et al. Rnn-based longitudinal analysis for diagnosis of alzheimer’s disease. *Computerized Medical Imaging and Graphics*, 73:1–10, 2019.
- [Dosovitskiy *et al.*, 2020] Alexey Dosovitskiy, Lucas Beyer, Alexander Kolesnikov, Dirk Weissenborn, Xiaohua Zhai, Thomas Unterthiner, Mostafa Dehghani, Matthias Minderer, Georg Heigold, Sylvain Gelly, et al. An image is worth 16x16 words: Transformers for image recognition at scale. *arXiv preprint arXiv:2010.11929*, 2020.
- [Eskildsen *et al.*, 2013] Simon F Eskildsen, Pierrick Coupé, Daniel García-Lorenzo, Vladimir Fonov, Jens C Pruessner, D Louis Collins, Alzheimer’s Disease Neuroimaging Initiative, et al. Prediction of alzheimer’s disease in subjects with mild cognitive impairment from the adni cohort using patterns of cortical thinning. *Neuroimage*, 65:511–521, 2013.

[Hu *et al.*, 2023] Zhentao Hu, Zheng Wang, Yong Jin, and Wei Hou. Vgg-tswinformer: Transformer-based deep learning model for early alzheimer’s disease prediction. *Computer Methods and Programs in Biomedicine*, 229:107291, 2023.

[Jack Jr *et al.*, 2008] Clifford R Jack Jr, Matt A Bernstein, Nick C Fox, Paul Thompson, Gene Alexander, Danielle Harvey, Bret Borowski, Paula J Britson, Jennifer L. Whitwell, Chadwick Ward, et al. The alzheimer’s disease neuroimaging initiative (adni): Mri methods. *Journal of Magnetic Resonance Imaging: An Official Journal of the International Society for Magnetic Resonance in Medicine*, 27(4):685–691, 2008.

[Jang and Hwang, 2022] Jinseong Jang and Dosik Hwang. M3t: Three-dimensional medical image classifier using multi-plane and multi-slice transformer. In *Proceedings of the IEEE/CVF Conference on Computer Vision and Pattern Recognition*, pages 20718–20729, 2022.

[Li *et al.*, 2018] Fan Li, Manhua Liu, Alzheimer’s Disease Neuroimaging Initiative, et al. Alzheimer’s disease diagnosis based on multiple cluster dense convolutional networks. *Computerized Medical Imaging and Graphics*, 70:101–110, 2018.

[Li *et al.*, 2022] Chao Li, Yue Cui, Na Luo, Yong Liu, Pier-rick Bourgeat, Jurgen Fripp, and Tianzi Jiang. Transresnet: Integrating transformers and cnns for alzheimer’s disease classification. In *2022 IEEE 19th International Symposium on Biomedical Imaging (ISBI)*, pages 1–5. IEEE, 2022.

[Lian *et al.*, 2018] Chunfeng Lian, Mingxia Liu, Jun Zhang, and Dinggang Shen. Hierarchical fully convolutional network for joint atrophy localization and alzheimer’s disease diagnosis using structural mri. *IEEE transactions on pattern analysis and machine intelligence*, 42(4):880–893, 2018.

[Lin *et al.*, 2017] Tsung-Yi Lin, Priya Goyal, Ross Girshick, Kaiming He, and Piotr Dollár. Focal loss for dense object detection. In *Proceedings of the IEEE international conference on computer vision*, pages 2980–2988, 2017.

[Lin *et al.*, 2018] Weiming Lin, Tong Tong, Qinquan Gao, Di Guo, Xiaofeng Du, Yonggui Yang, Gang Guo, Min Xiao, Min Du, Xiaobo Qu, et al. Convolutional neural networks-based mri image analysis for the alzheimer’s disease prediction from mild cognitive impairment. *Frontiers in neuroscience*, 12:777, 2018.

[Qiu *et al.*, 2020] Shangran Qiu, Prajakta S Joshi, Matthew I Miller, Chonghua Xue, Xiao Zhou, Cody Karjadi, Gary H Chang, Anant S Joshi, Brigid Dwyer, Shuhan Zhu, et al. Development and validation of an interpretable deep learning framework for alzheimer’s disease classification. *Brain*, 143(6):1920–1933, 2020.

[Qiu *et al.*, 2022] Anqi Qiu, Liyuan Xu, Chaoqiang Liu, Alzheimer’s Disease Neuroimaging Initiative, et al. Predicting diagnosis 4 years prior to alzheimer’s disease incident. *NeuroImage: Clinical*, 34:102993, 2022.

[Rezatofighi *et al.*, 2019] Hamid Rezatofighi, Nathan Tsoi, JunYoung Gwak, Amir Sadeghian, Ian Reid, and Silvio Savarese. Generalized intersection over union: A metric and a loss for bounding box regression. In *Proceedings of the IEEE/CVF conference on computer vision and pattern recognition*, pages 658–666, 2019.

[Rowe *et al.*, 2010] Christopher C Rowe, Kathryn A Ellis, Miroslava Rimajova, Pierrick Bourgeat, Kerryn E Pike, Gareth Jones, Jurgen Fripp, Henri Tochon-Danguy, Laurence Morandieu, Graeme O’Keefe, et al. Amyloid imaging results from the australian imaging, biomarkers and lifestyle (aibl) study of aging. *Neurobiology of aging*, 31(8):1275–1283, 2010.

[Saboo *et al.*, 2021] Krishnakant Saboo, Anirudh Choudhary, Yurui Cao, Gregory Worrell, David Jones, and Ravishankar Iyer. Reinforcement learning based disease progression model for alzheimer’s disease. *Advances in Neural Information Processing Systems*, 34:20903–20915, 2021.

[Shapey *et al.*, 2019] Jonathan Shapey, Guotai Wang, Reuben Dorent, Alexis Dimitriadis, Wenqi Li, Ian Padnick, Neil Kitchen, Sotirios Bisdas, Shakeel R Saeed, Sebastien Ourselin, et al. An artificial intelligence framework for automatic segmentation and volumetry of vestibular schwannomas from contrast-enhanced t1-weighted and high-resolution t2-weighted mri. *Journal of neurosurgery*, 134(1):171–179, 2019.

[Tong *et al.*, 2014] Tong Tong, Robin Wolz, Qinquan Gao, Ricardo Guerrero, Joseph V Hajnal, Daniel Rueckert, Alzheimer’s Disease Neuroimaging Initiative, et al. Multiple instance learning for classification of dementia in brain mri. *Medical image analysis*, 18(5):808–818, 2014.

[Touvron *et al.*, 2021] Hugo Touvron, Matthieu Cord, Matthijs Douze, Francisco Massa, Alexandre Sablayrolles, and Hervé Jégou. Training data-efficient image transformers & distillation through attention. In *International Conference on Machine Learning*, pages 10347–10357. PMLR, 2021.

[Vaswani *et al.*, 2017] Ashish Vaswani, Noam Shazeer, Niki Parmar, Jakob Uszkoreit, Llion Jones, Aidan N Gomez, Łukasz Kaiser, and Illia Polosukhin. Attention is all you need. *Advances in neural information processing systems*, 30, 2017.

[Wu *et al.*, 2022] Junfeng Wu, Yi Jiang, Song Bai, Wenqing Zhang, and Xiang Bai. Seqformer: Sequential transformer for video instance segmentation. In *European Conference on Computer Vision*, pages 553–569. Springer, 2022.

[Zhang *et al.*, 2022] Shengjie Zhang, Xiang Chen, Bohan Ren, Haibo Yang, Ziqi Yu, Xiao-Yong Zhang, and Yuan Zhou. 3d global fourier network for alzheimer’s disease diagnosis using structural mri. In *International Conference on Medical Image Computing and Computer-Assisted Intervention*, pages 34–43. Springer, 2022.

[Zheng *et al.*, 2021] Sixiao Zheng, Jiachen Lu, Hengshuang Zhao, Xiatian Zhu, Zekun Luo, Yabiao Wang, Yanwei Fu, Jianfeng Feng, Tao Xiang, Philip HS Torr, et al.

Rethinking semantic segmentation from a sequence-to-sequence perspective with transformers. In *Proceedings of the IEEE/CVF conference on computer vision and pattern recognition*, pages 6881–6890, 2021.

[Zhu *et al.*, 2020] Xizhou Zhu, Weijie Su, Lewei Lu, Bin Li, Xiaogang Wang, and Jifeng Dai. Deformable detr: Deformable transformers for end-to-end object detection. *arXiv preprint arXiv:2010.04159*, 2020.

[Zhu *et al.*, 2021] Wenyong Zhu, Liang Sun, Jiashuang Huang, Liangxiu Han, and Daoqiang Zhang. Dual attention multi-instance deep learning for alzheimer’s disease diagnosis with structural mri. *IEEE Transactions on Medical Imaging*, 40(9):2354–2366, 2021.